Re-engineering lysozyme solubility and activity through surfactant complexation

Jiaming Mu[a], Leran Mao[b], Gavin Andrews[a], Sheiliza Carmali *[a]

[a] School of Pharmacy, Queen's University Belfast, BT9 7BL Belfast, United Kingdom

E-mail: s.carmali@qub.ac.uk

[b] Department of Chemical Engineering, Carnegie Mellon University, Pittsburgh, Pennsylvania, 15213, United States

Supporting Information

Lysozyme-surfactant ion pairing at different pH. Lysozyme was ion paired with 3.1 mM SDS solution at pH 2, 4, 6, 9 and 11. Complexation efficiency was determined by Micro BCA assay. The highest complexation efficiency was achieved at pH 4.

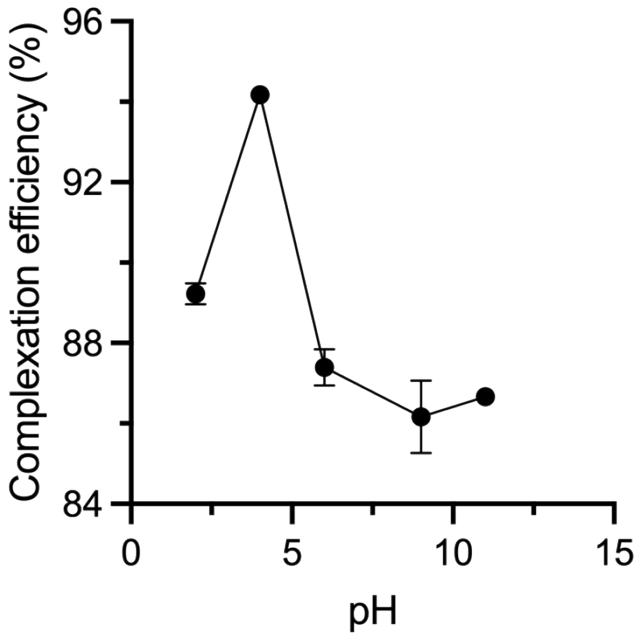

Supplementary Figure S1. Graphical representation of the complexation efficiency of lysozyme at pH 2, 4, 6, 9 and 11.

Lysozyme-surfactant dissociation. Lysozyme-surfactant complex was incubated in 50 mM phosphate buffer, pH 6.5 with 0.1, 0.5, or 1 M NaCl at a concentration of 1 mg/mL. H_2O was used as blank control. Samples were vortexed at 550 rpm for 3 h at 37 ℃, then centrifuged at 13,500 rpm for 10 min. Subsequently, an aliquot of 50 μL supernatant was withdrawn and amount of dissociated protein in supernatant was quantified with Micro BCA assay. The percentage of dissociated protein was calculated by Eq. (3).

$$Dissociation\ (\%) = \left(\frac{C_{lysozyme\ in\ supernatant}}{C_{initial\ lysozyme\ in\ HIP}}\right) \times 100 \quad (3)$$

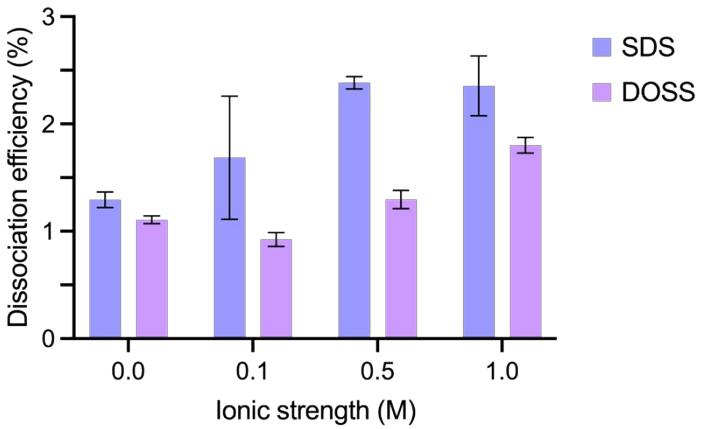

Supplementary Figure S2. Lysozyme-surfactant dissociation study carried out at 0.1, 0.5 and 1.0 M NaCl.

Critical micelle concentration (CMC) determination for SDS and DOSS. Methodology was adopted from Perinelli, D. R. *et al*.[1] Twenty µL, 3 µM of pyrene solution in methanol were added to the aqueous surfactant solutions. Pyrene spectrum in the excitation wavelength of 334 nm was recorded between 220 and 700 nm with an excitation and emission slit of 2.5 nm. Measurement was performed with HITACHI F-2710 fluorescence spectrophotometer at room temperature. The ratio of emission spectrum peak intensity I (λ = 372 nm) to peak intensity III (λ = 384 nm) were plotted against surfactant concentration. Data points were interpolated by cubic basis spline method using Origin Pro 2023b. The second derivative of the interpolated curve was calculated. CMC values were determined based on the maximum point of the second derivative from each surfactant *vs* concentration plot. The results showed the CMC value of 7.2 mM for SDS, and 4.8 mM for DOSS.

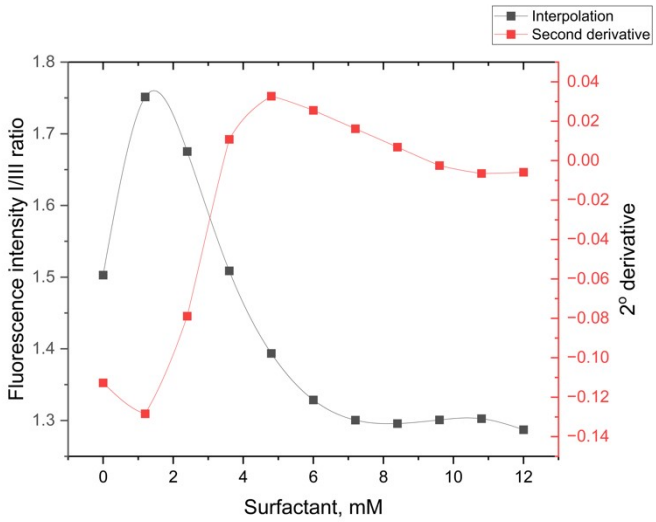

Supplementary Figure S3. Fluorescence intensity (peak I/III) *vs* concentration plots for SDS.

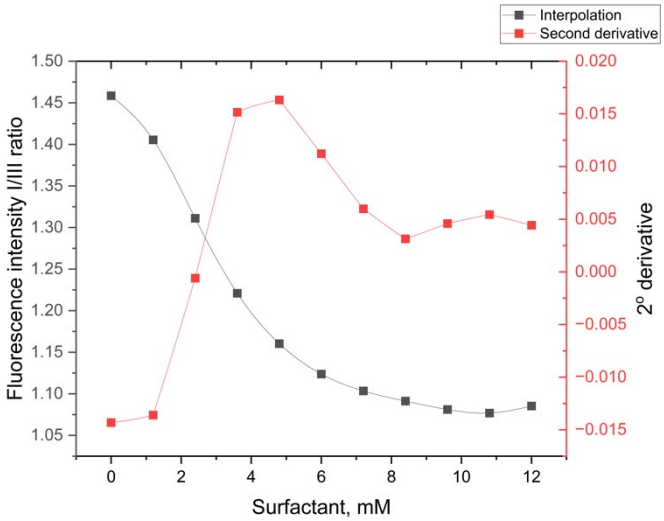

Supplementary Figure S4. Fluorescence intensity (peak I/III) *vs* concentration plots for DOSS.

Supplementary Table S1. Average particle size (nm) of lysozyme-SDS or lysozyme-DOSS complexes, as measured by dynamic light scattering, at a fixed concentration of 10 mg/mL.

	Particle size (nm)
Native lysozyme	1.44 ± 0.06
L-SDS 4:1	1.93 ± 0.06
L-SDS 2:1	2.70 ± 0.21
L-SDS 1:1	138.2 ± 47.3
L-SDS 1:2	170.1 ± 29.7
L-SDS 1:4	2.19 ± 0.09
L-DOSS 4:1	1.89 ± 0.08
L-DOSS 2:1	2.58 ± 0.13
L-DOSS 1:1	95.21 ± 9.18
L-DOSS 1:2	117.5 ± 60.0
L-DOSS 1:4	91.58 ± 19.5

Supplementary Table S2. Weight of the native lysozyme and lysozyme-surfactant complexes used for differential scanning calorimetry study.

Sample	Weight (mg)
Lysozyme 01	4.81
Lysozyme 02	5.51
Lysozyme 03	3.59
SDS 0.8 mM 01	0.45
SDS 0.8 mM 02	0.21
SDS 0.8 mM 03	0.23
SDS 1.6 mM 01	1.28
SDS 1.6 mM 02	1.08
SDS 1.6 mM 03	1.13
SDS 3.1 mM 01	3.20
SDS 3.1 mM 02	2.06
SDS 3.1 mM 03	3.11
SDS 6.3 mM 01	3.24
SDS 6.3 mM 02	3.97
SDS 6.3 mM 03	3.81
SDS 12.5 mM 01	3.44
SDS 12.5 mM 02	3.17
SDS 12.5 mM 03	3.35
DOSS 0.8 mM 01	4.21
DOSS 0.8 mM 02	3.47
DOSS 0.8 mM 03	3.61
DOSS 1.6 mM 01	4.31
DOSS 1.6 mM 02	0.52
DOSS 1.6 mM 03	4.00

DOSS 3.1 mM 01	2.22
DOSS 3.1 mM 02	2.25
DOSS 3.1 mM 03	2.59
DOSS 6.3 mM 01	6.19
DOSS 6.3 mM 02	6.78
DOSS 6.3 mM 03	5.23
DOSS 12.5 mM 01	5.91
DOSS 12.5 mM 02	6.34
DOSS 12.5 mM 03	5.47

Molecular Dynamics Trajectory Analysis

To investigate the source of catalytic enhancement of lysozyme with surfactant addition, we recreated our experimental system *in silico* using molecular dynamics (MD) simulation with lysozyme protonated at pH 6.5. To mimic the exact experimental conditions, we neutralized and solvated lysozyme with 50 mM K^+ and PO_3^{2-} ions. To represent the most pronounced difference between SDS and DOSS's effect on lysozyme activity, we chose to add 9 stoichiometric ratios of either surfactant to lysozyme in our simulation. At this stoichiometry, SDS increased lysozyme activity, yet DOSS resulted in no significant increase in activity compared to native lysozyme. As a comparison, we also chose a condition of 25 stoichiometric ratios of SDS added to lysozyme to represent a case where lysozyme activity is fully lost. After the production run, the RMSD of the simulation is shown in **Supplementary Figure S5.**, for all experimental systems, the protein backbone is relatively stabilized after 35 ns in an NPT production ensemble.

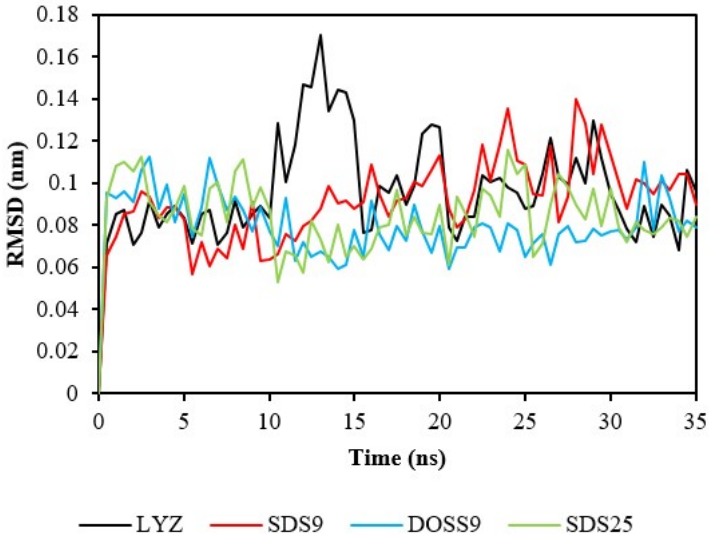

Supplementary Figure S5. Root-mean-squared deviation (RMSD) of tested experimental conditions. The black, red, blue, and green lines represent native lysozyme, lysozyme with 9 stoichiometric ratios of SDS molecules, lysozyme with 9 stoichiometric ratios of DOSS molecules, and lysozyme with 25 stoichiometric ratios of SDS molecules.

To delve into the origin of enhanced activity, we first analysed the 'openness' of the active site by measuring the distance between two active site residues in lysozyme, GLU35, and ASP52. Mechanistically, ASP52 establishes a partial bond to the saccharide backbone of sugars, and GLU35 accepts an electron, leading to the NAG leaving group while ASP52 stabilizes the catalytic reaction intermediate structure. Finally, GLU35 donates an electron to water, and ASP52 re-establishes the full bond to create a hydrolysed saccharide product, completing the catalytic cycle.[2] Therefore, the roles of GLU35 and ASP52 are essential. Our analysis did not show a significant difference in inter-residue distance between GLU35 and ASP52 of all analysed structures (**Supplementary Figure S6**).

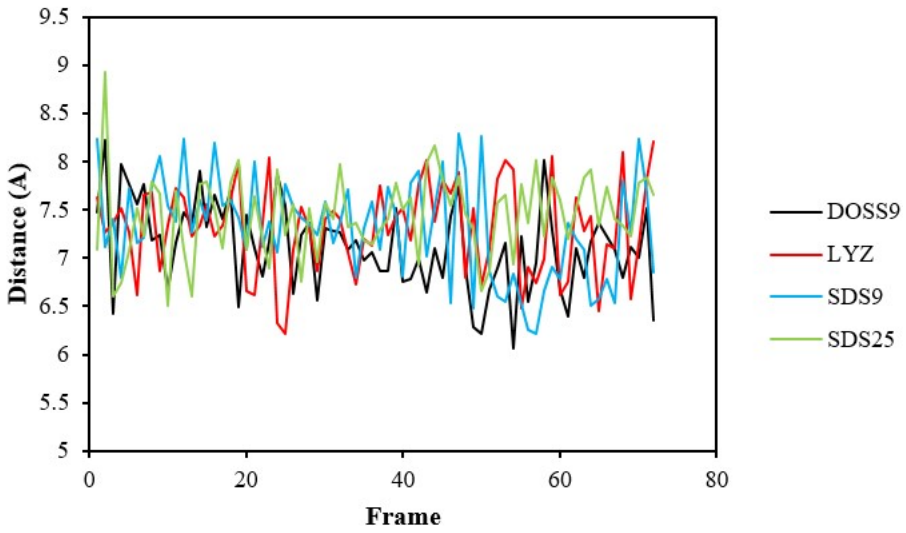

Supplementary Figure S6 Distance between the active site residues GLU35 and ASP52. The carboxylate ends of both residuals were used as a reference for the calculation. The black, red, blue, and green lines represent native lysozyme, lysozyme with 9 stoichiometric ratios of SDS molecules, lysozyme with 9 stoichiometric ratios of DOSS molecules, and lysozyme with 25 stoichiometric ratios of SDS molecules. The frames are representative of the entire simulation.

However, we found there is a higher degree of backbone flexibility of the GLU35 and ASP52 residues compared to the initial simulation frame (the initial position) when 9 stoichiometric ratios of SDS were added (**Supplementary Figure S7**), suggesting SDS likely increased active site flexibility, leading to a higher possibility of exposure to the incoming saccharide molecules. Crucially, the active site flexibility mobility is highly correlated with lysozyme biological activity.[3]

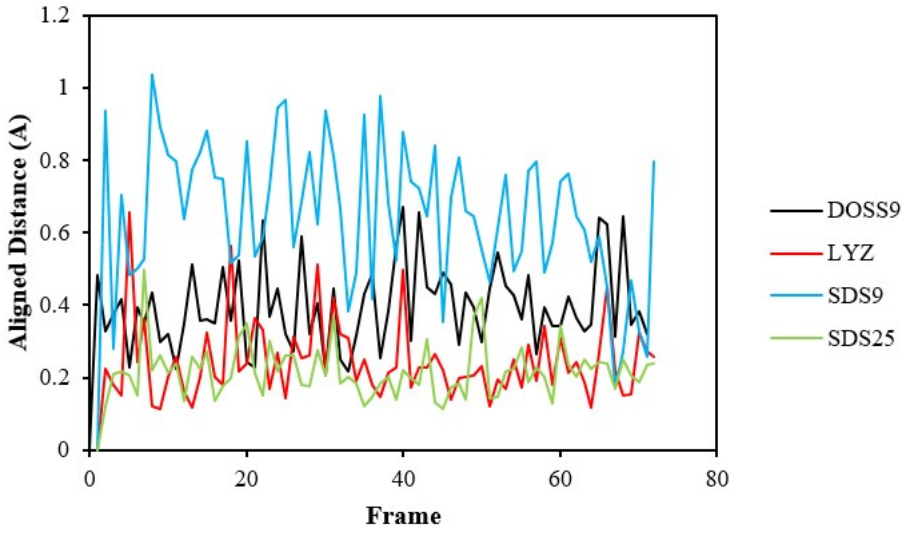

Supplementary Figure S7 Aligned root mean squares deviation (RMSD) of the active site residue GLU35 and ASP52 backbones. The black, red, blue, and green lines represent native lysozyme, lysozyme with 9 stoichiometric ratios of SDS molecules, lysozyme with 9 stoichiometric ratios of DOSS molecules, and lysozyme with 25 stoichiometric ratios of SDS molecules. The frames are representative of the entire simulation.

Following this thought, we continued to analyse the radial distribution function of the active site residues GLU35 and ASP52 to nearby water molecules, as well as the solvent-exposed surface area (SASA) of the respective protein conformations. As expected, lysozyme with 9 ratios of SDS showed a selective enhancement of hydration, especially from the second hydration shell onwards (**Supplementary Figure S8**). This likely implies that the addition of SDS does not interfere with direct hydrogen bond formation, but stabilizes hydrogen bonds by altering protein conformation, thereby increasing water dynamics to the active site residue to support both the catalytic reaction via water exchange (where water is a necessary reaction component) and result in a more compact water shell. Notably, lysozyme with 25 SDS molecules showed a decrease in hydration, suggesting a possible route of activity loss. On the other hand, the hydration of ASP52 did not show noticeable differences in all conditions, despite native lysozyme showing a slightly increased hydration in the adjacent solvent phase.

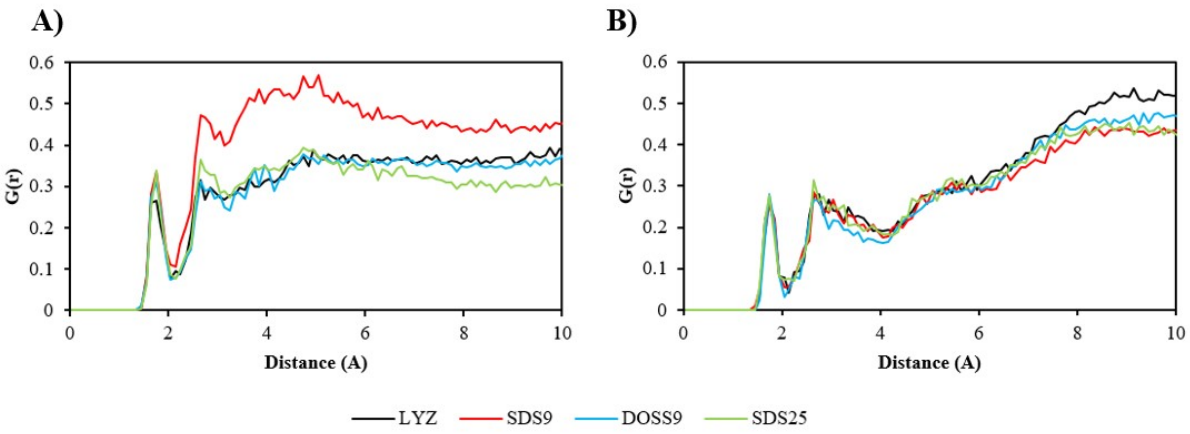

Supplementary Figure S8 Radial distribution function (G(r)) of explicit water molecules from the two active sites of the catalytic pocket, **A)** GLU35 and **B)** ASP52. The black, red, blue, and green lines represent native lysozyme, lysozyme with 9 stoichiometric ratios of SDS molecules, lysozyme with 9 stoichiometric ratios of DOSS molecules, and lysozyme with 25 stoichiometric ratios of SDS molecules. The results are representative of the entire simulation.

In addition, only lysozyme with 9 ratios of SDS showed an increased SASA in the active site residue GLU35, whereas the other tested conditions did not show a significant difference. Interestingly, the SASA of ASP52 again showed no difference among all conditions tested, suggesting the enhanced activity effect primarily stemmed from alternations in GLU35 conformation. Therefore, we analysed the secondary structure of the tested conditions. Surprisingly, lysozyme with 9 ratios of SDS showed predominantly a β-turn secondary structure of GLU35 throughout the simulation, whereas the other conditions demonstrated an α-helix structure at the GLU35 site (**Supplementary Figure S9**). The β-turn structure has been shown to increase protein stability and dynamics[4,5], and increases solvent exposure. Again, no difference was shown for the ASP52 site. Overall, our results suggested SDS likely altered the secondary structure of the lysozyme active site by modulating the active site's backbone flexibility, leading to higher levels of exposure to catalytic reaction components.

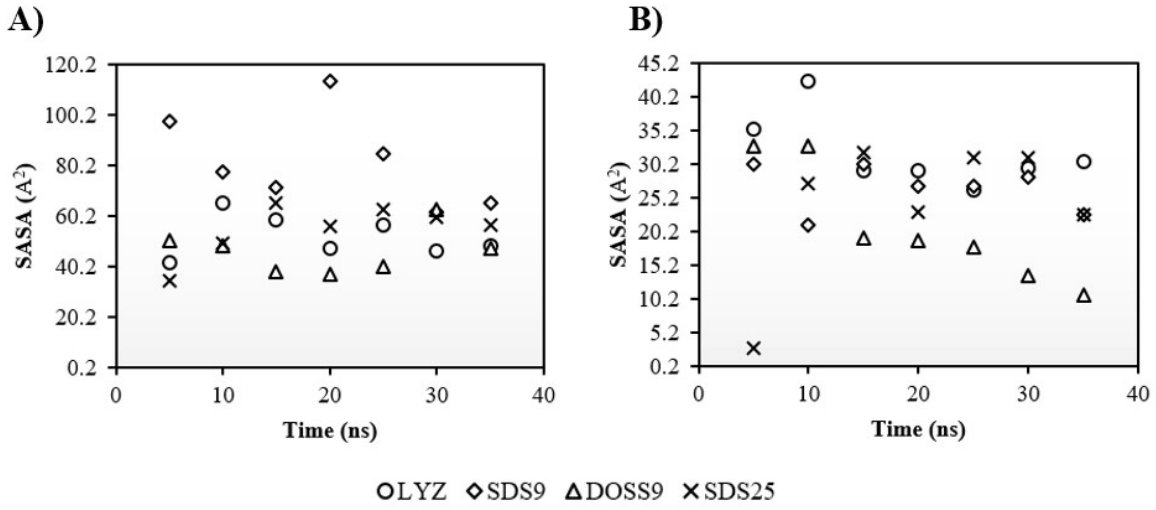

Supplementary Figure S9 Solvent exposed surface area (SASA) of the two active sites of the catalytic pocket, **A)** GLU35 and **B)** ASP52. The circle, diamond, triangle, and cross symbols represent native lysozyme, lysozyme with 9 stoichiometric ratios of SDS molecules, lysozyme with 9 stoichiometric ratios of DOSS molecules, and lysozyme with 25 stoichiometric ratios of SDS molecules. The average protein structures from each 5 ns simulation were analysed from the entire 35 ns simulation.

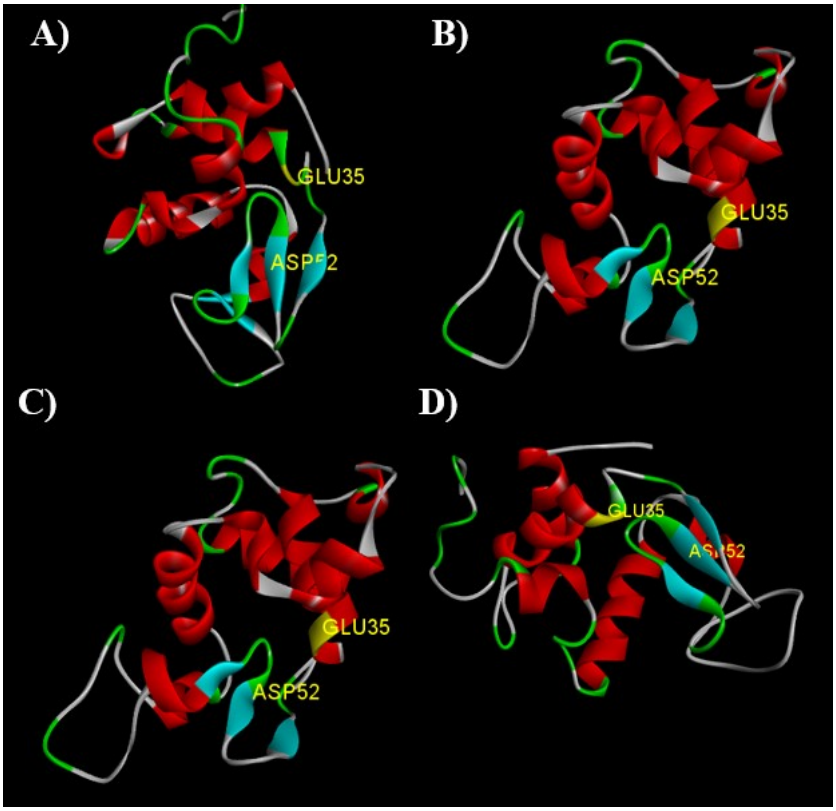

Supplementary Figure S10. The secondary structure of the active site GLU35 changed only with 9 stoichiometric ratios of SDS. The protein structures were shown for the averaged structure of **A)** lysozyme with 9 ratios of SDS, **B)** native lysozyme, **C)** lysozyme with 9 ratios of DOSS, and **D)** lysozyme with 25 stoichiometric ratios of SDS during 15-20 ns of the MD run. Surfactants are not shown for better visualization of the protein structure.

REFERENCES

1. Perinelli, D. R., Cespi, M., Lorusso, N., Palmieri, G. F., Bonacucina, G., and Blasi, P., “Surfactant self-assembling and critical micelle concentration: one approach fits all?,” *Langmuir* vol. 36, pp. 5745–5753, 2020.
2. A. J. Kirby, "The lysozyme mechanism sorted — after 50 years," *Nature Structural Biology,* vol. 8, pp. 737-739, 2001.
3. P. J. Artymiuk, C. C. Blake, D. E. Grace, S. J. Oatley, D. C. Phillips and M. J. Sternberg, "Crystallographic studies of the dynamic properties of lysozyme," *Nature,* vol. 280, no. 5732, pp. 563-568, 1979.
4. K. Fujiwara, S. Ebisawa, Y. Watanabe, H. Fujiwara and M. Ikeguchi, "The origin of β-strand bending in globular proteins," *BMC Structural Biology,* vol. 15, 2015.
5. B. Halle, "Flexibility and packing in proteins," *Biophysics and Computational Biology,* vol. 99, no. 3, pp. 1274-1279, 2002.